Structure and Melt Rheology of Long-Chain Branching Polypropylene/Clay Nanocomposites

Feng-Hua Su, Jia-Hua Yan, Han-Xiong Huang

Center for Polymer Processing Equipment and Intellectualization, School of Mechanical and Automotive Engineering, South China University of Technology, Guangzhou 510641, People's Republic of China

Received 14 March 2010; accepted 13 May 2010
DOI 10.1002/app.32800
Published online 2 August 2010 in Wiley Online Library (wileyonlinelibrary.com).

ABSTRACT: Long-chain branching polypropylene (LCB-PP)/clay nanocomposites were prepared by melt blending in a twin-screw extruder. The microstructure and melt rheology of these nanocomposites were investigated using x-ray diffraction, transmission electron microscopy, oscillatory shear rheology, and melt elongation testing. The results show that, the clay layers are intercalated by polymer molecular chains and exfoliate well in LCB-PP matrix in the presence of maleic anhydride grafted PP. Rheological characteristics, such as higher storage modulus at low-frequency and solid-like plateau in tan-ω curve, indicate that a compact and stable filler network structure is formed when clay is loaded at 4 phr (parts per hundred parts of) or higher. The response of the nanocomposite under melt extension reveals an initial decrease in the melt strength and elongational viscosity with increasing clay concentration up to 6 phr. Later, the melt strength and elongational viscosity show slight increases with further increasing clay concentration. These results might be caused by a reduction in the molecular weight of the LCB-PP matrix and by the intercalation of LCB-PP molecular chains into the clay layers. Increases in the melt strength and elongational viscosity for the nanocomposites with decreasing extrusion temperature are also observed, which is due to flow-induced crystallization under lower extrusion temperature. © 2010 Wiley Periodicals, Inc. J Appl Polym Sci 119: 1230–1238, 2011

Key words: long-chain branching polypropylene; nanocomposites; structure; rheology

INTRODUCTION

Polypropylene (PP) is the fastest growing resin commodity in the polymer world market, because of its desirable and beneficial physical properties, such as its stiffness, resistance to corrosive chemicals, lack of non environmental pollution when incinerated, and low-specific gravity. However, commercial PP produced with metallocene catalyst has a linear molecular structure with a narrow molecular weight distribution, which leads to the linear PP having relative low-melt strength and exhibiting no strain hardening behavior in the melt state. Compared with linear PP, long-chain branching polypropylene (LCB-PP) possesses many advantageous properties that are important in many industrial applications such as thermoforming, foaming, and blow molding.[1,2] One way to create LCB in linear PP is modification by a reactive extrusion process.[3–6] The authors previously prepared LCB-PP by reactive extrusion in the presence of peroxide and polyfunctional monomer.[5] In addition to the LCB structure, some filler materials, such as carbon nonotube, talc, and clay, were found to improve the elongational viscosity and melt strength of linear PP.[7–10] Mcinerney et al.[7] investigated the melt strength and extensibility of talk-filled polypropylene and found that the melt strength of the PP was decreased for talc additions of less than 40 wt % under all test conditions. However, the addition of 50 wt % talc can improve the melt strength under all testing conditions. Moreover, they found that the drawability of PP decreased with increased filler loading and the melt strength of all materials decreased with increased temperature. However, the influence of mineral filler on the melt strength and rheological characteristics, especially the melt extension, of LCB-PP has not been studied even though LCB-PP possesses many advantageous merits compared with linear PP.

During the last 10 years, the development of polymer/clay nanocomposites[11–15] has gained increasing interest, becoming one of the most important research topics in the area of polymer-based composite technology. The addition of clay into PP has been considered an effective means for improving tensile moduli, thermal stability, electronic conductivity, and gas barrier properties. During the preparation of polymer/clay

Correspondence to: F.-H. Su (fhsu@scut.edu.cn).
Contract grant sponsor: The National Natural Science Foundation of China; contract grant number: 20904012.
Contract grant sponsor: The Fundamental Research Funds for the Central Universities; contract grant number: 2009ZM0157.

nanocomposites, the particles of clay are driven to undergo intercalation and exfoliation processes. In addition to its effect on solid-state polymer properties, clay's influence on melt rheology of the polymer must be carefully considered. The addition of clay can induce a change in the melt rheology of the polymer, which may result in processing behavior, is unacceptable for the desired application. Research on the influence of clay on the shear rheology of filled linear PP is relatively common because the rheological characteristics are directly related to the structure and properties of the nanocomposites.[16–18] However, compared to the shear rheology, studies on the effect of fillers on melt extension of polymers have not been active in the past decades even though the melt extension is often encountered in many polymer processes, including blow molding, vacuum foaming, melt spinning, and foaming.

As illustrated above, the extensibility of the polymer melt is of great importance for many polymer processes. Extensibility can be determined by an "extension diagram," where the drawdown force needed for elongation of an extruded strand is measured as a function of slowly increasing drawdown speed. For this purpose, a tensile tester, the so-called "Rheotens," was developed, which probes a whole set of melt spinning conditions in one test run.[19–21] The analysis of this complicated deformation history is simplified by the existence of "Rheotens Grandmastercurves."[21–23] These curves allow for a direct and straightforward description of material behavior in the fiber spinning process and a simplified determination of an apparent elongational viscosity under the action of a constant drawdown force. A number of studies on melt elongational behavior of filled polymers have been performed.[7–10,24–27] In the present contribution, LCB-PP/clay nanocomposites were prepared by melt blending in a twin-screw extruder, and the LCB-PP was obtained by reactive extrusion in the presence of peroxide and polyfunctional monomer. The microstructure, oscillatory shear rheology, and melt extension for the LCB-PP based nanocomposites containing varied mass fractions of clay were focused on in this study. Moreover, this work also attempted to investigate the correlations between the structures' melt viscoelastic behavior and melt elongational behavior for the prepared nanocomposites.

EXPERIMENTAL

Materials

Commercially available isotactic PP (trademarked as MPHM160, Mao Ming Petroleum of China) with a melt flow index of 21.0 g/10 min was used as linear PP for the preparation of the LCB-PP. The peroxide and multifunctional monomer were dibenzoyl peroxide from Lanzhou Auxiliary Agent Plant, China, and 1, 6-hexanediol diacrylate from Tianjintianjiao Chemical (China), respectively. The clay is a commercial organic montmorillonite (Nanomer 1.44P from Nanocor) that has been modified with dimethyl dialkyl ammonium halide. A thermogravimetric analysis performed on the clay shows that, it contains 26 wt % organic material. PP-g-MA is a commercial maleic anhydride grafted polypropylene (trade name PP-G-4) provided by Nanjing Deba Chemical (China).

Preparation of LCB-PP/clay nanocomposites

The LCB-PP/clay nanocomposites were prepared by two processes. The first process is the preparation of LCB-PP by modifying linear PP in the presence of peroxide and monomer by reactive extrusion. The concentrations of peroxide and monomer, used to add long branched chains onto linear PP backbone, were 3.0 phr and 400 ppm, respectively. The modified processes have been reported in authors' previous research.[5] The prepared LCB-PP and PP-g-MA were used as the base polymers. The second process is as follow. The mixing of LCB-PP, PP-g-MA, and clay in an SHR10A high-speed mixer was maintained for 10 min followed by melt blending in a TE35 co-rotating twin-screw extruder. The temperature of the extruder was maintained between 170–210°C from hopper to die. The throughput and the screw speed were 6.0 kg/h and 120 rpm, respectively. The compositions of LCB-PP, PP-g-MA, and clay and their abbreviations for these nanocomposites are shown in Table I.

Characterization

X-ray diffraction (XRD) experiments were carried out with a Rigaku (Japan) D/max-IIIA diffractometer. The X-ray beam was derived from nickel-filtered CuK ($\lambda = 0.154$ nm) radiation in a sealed tube operated at 40 kV and 30 mA. The test samples were prepared by compression molding. The experiments were performed in the angle range of 2°–10°, at a scanning step of 0.02°/s.

The nanocomposite samples for transmission electron microscopy (TEM) examination of nanocomposites were prepared by ultramicrotome at −60°C using an ultramicrotome equipped with a diamond knife. The microscopic study was conducted with a JEOL (JEM-100CXII) transmission electron microscope.

Small-amplitude oscillatory shear rheology measurements were conducted with a Bohlin Gemini 200 rheometer equipped with a parallel-plate fixture (25-mm diameter). Disk-shaped samples were prepared by compression molding to a thickness of 2.0 mm and a diameter of 25 mm. The gap between the two

TABLE I
Compositions and Abbreviations of the Prepared Nanocomposites

	Composition (weight fraction)			
Abbreviation	Linear PP	LCB-PP	PP-g-MA	Clay
PP1	100		0	0
PP2		100	0	0
PP3		95	5	0
PP4		95	5	2
PP5		95	5	4
PP6		95	5	6
PP7		95	5	8
PP8		95	5	10

parallel plates was maintained at 1.75 mm for all measurements. The measurements were performed as a function of angular frequency (ω) ranging from 0.01 to 100 rad/s at 190°C. A fixed strain of 1% was used to ensure that all measurements were carried out within the linear viscoelastic range of the materials.

The melt extension was performed using a Rheotens-apparatus developed by Meissner,[19] which is an established scientific and industrially used method for the characterization of the melt extension behavior. As shown in Figure 1, the experimental set-up for Rheotens measurements includes a device that continuously provides an extruded melt strand, in the present case, a high-pressure capillary rheometer (Rheograph 25, GÖttfert), combined with the Rheotens-apparatus (Rheotens 71.97, GÖttfert) for the uniaxial elongation of the melt. Using a tubular die (diameter 1 mm, length 30 mm) and a constant piston speed of the capillary rheometer (0.05 mm/s), the melt strand was supplied at an average die exit velocity of 11.3 mm/s (at a shear rate of 90 s^{-1}). The melt strand is subsequently fed to the Rheotens unit and was continuously drawn down between the two counter-rotating wheels of the device, mounted on a balanced beam. The distance between the die and the wheels was set at 100 mm. The starting velocity of the wheels was adjusted to the die exit velocity of the melt strand. The speed of the wheels was linearly accelerated at 12.0 mm/s^2 until rupture of the melt strand occurred.

The draw-down force was continuously measured as a function of the angular speed of the wheels. The force and velocity (draw ratio) measured when the melt strand was broken were deemed as "melt strength" and "drawability," respectively, at the tested conditions. The obtained force–velocity curves were converted to elongational viscosity–elongation rate curves by fitting the experimental Rheotens data by applying the analytical Wagner model.[21–23] The materials of PP1-PP8 were investigated at a constant temperature of 190°C. PP8 was selected as a case to investigate the influence of extrusion temperature (180–210°C) on the melt extension of the nanocomposites.

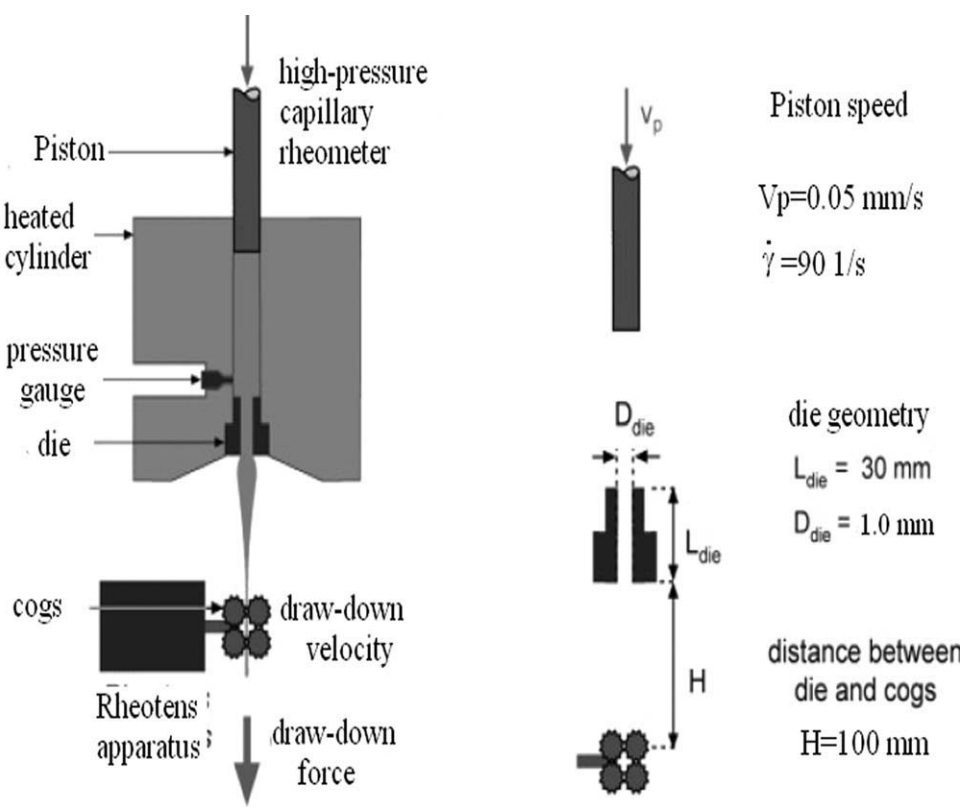

Figure 1 Experimental rheotens set-up for evaluating the melt elongational behavior of polymer.

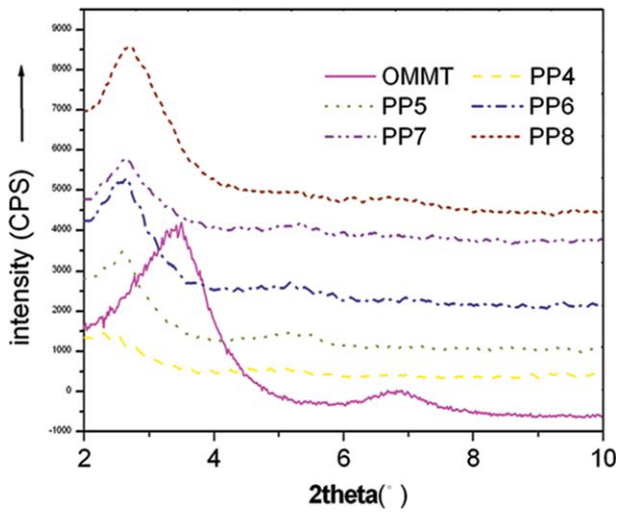

Figure 2 XRD patterns of primary clay and LCB-PP/clay nanocomposites. [Color figure can be viewed in the online issue, which is available at wileyonlinelibrary.com.]

RESULTS AND DISCUSSION

Dispersion morphology of layered clay in nanocomposites

Figure 2 exhibits the XRD patterns of clay and LCB-PP/clay nanocomposites with the peak-fitting scheme. The d001 spacing is calculated from Bragg's law. The interlayer distances for clay and nanocomposites for PP4-PP8 are listed in Table II. As shown in Figure 2, the clay exhibits a strong peak at a diffraction angle of $2\theta = 3.48°$, corresponding to an interlayer spacing of 2.53 nm for primary clay. The d-spacing is enlarged from 2.53 nm for primary clay to 3.28 nm ($2\theta = 2.70°$) or more for nanocomposites, suggesting that LCB-PP molecular chains intercalate the clay layer and increase the gallery distance of clay during melt-compounding. Figure 2 also shows that PP4 has a very weak peak, which suggests a exfoliated structure existing in PP4 at low-clay loadings (2 phr). And dramatic enhancements in peak intensity are observed as the clay content increase from 2 (PP4) to 10 phr (PP8). Table II shows that the d-spacing is reduced from 3.85 nm ($2\theta = 2.30°$) for PP4 to 3.28 nm ($2\theta = 2.70°$) for PP8, which indicates that the interlayer distance of clay in nanocomposites slightly decreases with increasing clay loadings. The result might be due to the clay tactoids at higher concentration levels of clay, which is also confirmed by supplementary TEM analysis.

To qualitatively understand the internal structure of the nanocomposites and to examine the dispersion level of the clay in the LCB-PP matrix, TEM analysis is carried out to complement the structure analysis from XRD results. Figure 3 represents the micrographs corresponding to the LCB-PP based nanocomposites filled with 2, 6, and 10 phr clay (PP4, PP6, and PP8). The images are obtained with a magnification of 1,00,000. As shown in Figure 3(a), at low-clay contents, e.g., 2 phr, most of clay is exfoliated in the matrix. Consequently, observed single platelets reveal lateral dimensions of about 100–200 nm and thicknesses of about 2–5 nm. The results agree with the XRD analysis showing d-spacing of 3.85 nm for PP4. However, in comparison with PP6 and PP10, the density of clay in PP4 is too low, which is attributed to low-level of clay in PP4. In the case of PP6 [Fig. 3(b)], a larger density of particles of different sizes is observed when compared to PP4, which is in agreement with the XRD results. Clay particles are well dispersed in the LCB-PP matrix, and the aggregation of clay particles is undetectable. At higher clay content of 10 phr [Fig. 3(c)], the density of clay is much larger than that of PP4 and PP6. However, the thickness of some exfoliated clay flack in PP8 increases and few clay particles are dispersed in the matrix as tactoids, indicating that excessive clay in the system is harmful to the exfoliation of clay in the LCB-PP matrix. The micrograph shown in Figure 3(c) demonstrates that the most of the clay is intercalated by the LCB-PP molecular chain, which is also quantitatively confirmed by d-spacing values of 3.28 nm for PP8. Therefore, TEM analysis provides complementary results for XRD analyzes to validate the remarkablely intercalated and mostly exfoliated structure in such nanocomposites.

Oscillatory shear rheology of the nanocomposites

Rheology is a powerful tool for inspecting the internal microstructure of polymer nanocomposites containing intercalated and/or exfoliated clay nanoparticles. The topic of linear PP/clay interactions has received a great deal of attention in polymer/clay-based systems. Fu and coworkers[12] investigated the shear response and disorientation kinetics of the molten linear PP/clay nanocomposites through oscillatory shear measurements and stress relaxation experiment. Quinzani and coworkers[16] evaluated the influence of the concentration of clay or the concentration ratio of PP-g-MA/clay on the structure of linear PP/clay nanocomposites by their linear viscoelastic

TABLE II
Interlayer Spacing of Clay in Nanocomposites Determined by XRD

Sample	2θ/(°)	d001/nm
clay	3.94	2.24
PP4	2.30	3.85
PP5	2.56	3.42
PP6	2.62	3.35
PP7	2.66	3.34
PP8	2.70	3.28

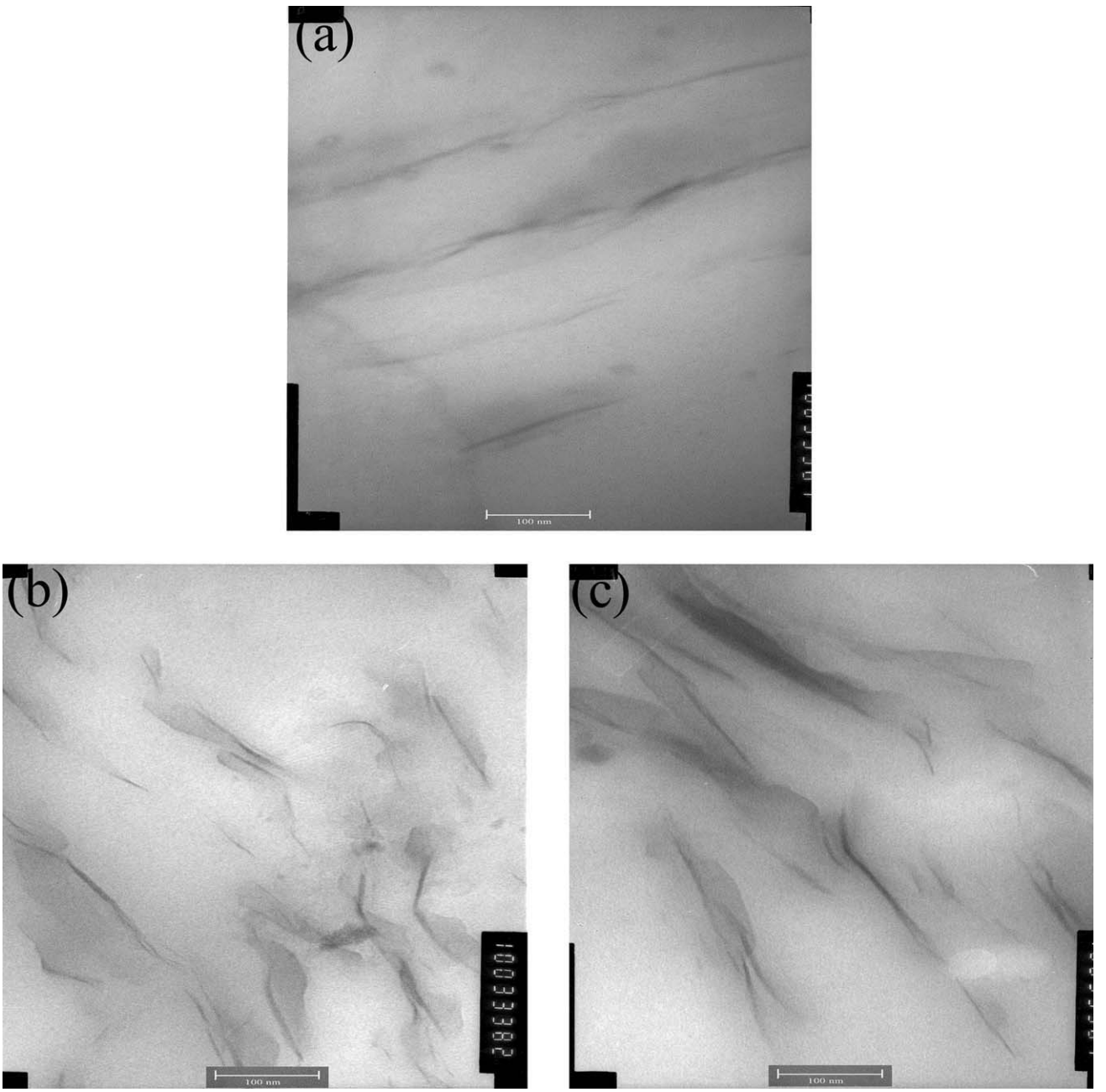

Figure 3 TEM images of LCB-PP based nanocomposites filled with 2 wt % clay (a), 6 wt % clay (b), and 10 wt % clay (c).

properties. In this section, oscillatory shear rheology is employed to investigate the structure characteristics of the LCB-PP/clay nanocomposites and their linear viscoelastic properties.

The storage modulus (G'), complex viscosity (η^*), and tangent of loss angle ($\tan \delta = G''/G'$) for linear PP, LCB-PP, LCB-PP/PP-g-MA blends, and LCB-PP/clay nanocomposites plotted as a function of frequency (ω) are shown in Figures 4–6, respectively. As shown in Figure 4, the linear PP exhibits typical terminal behavior in the G' *vs.* ω curve beccause of its linear chain structure. However, the typical terminal behavior is not observed for PP2, and, in comparison with PP1, as shown in Figure 5, PP2 has a higher shear viscosity and shows typical shear-shinning behavior. The curve of $\tan \delta$ *vs.* ω, as shown in Figure 6, is ascending with frequency for PP1, which is typical terminal behavior of liquid-like material. However, the $\tan \delta$ decreases quickly at low-frequency and shows a typical plateau for PP2. It is clear from these linear viscoelastic plots that a longer relaxation process appears in PP2, which is caused by long-chain branching in its backbone. Many researchers, including ours previous research,[5] have reported similar linear viscoelastic behavior of LCB-PP.[3,4]

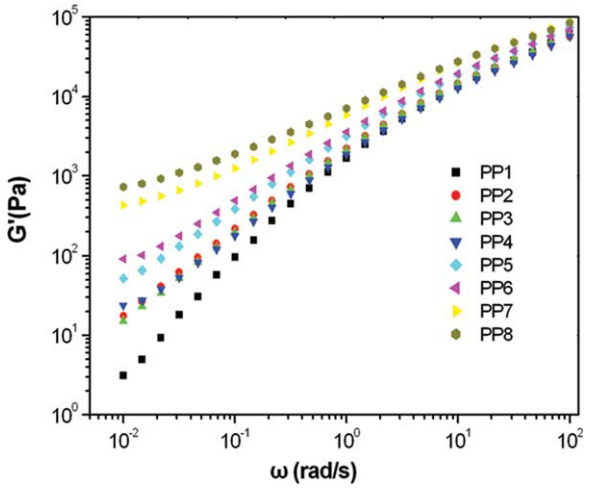

Figure 4 G' vs. ω of linear PP, LCB-PP, LCB-PP/PP-g-MA blends, and LCB-PP/clay nanocomposites with varied clay concentrations at 190°C. [Color figure can be viewed in the online issue, which is available at wileyonlinelibrary.com.]

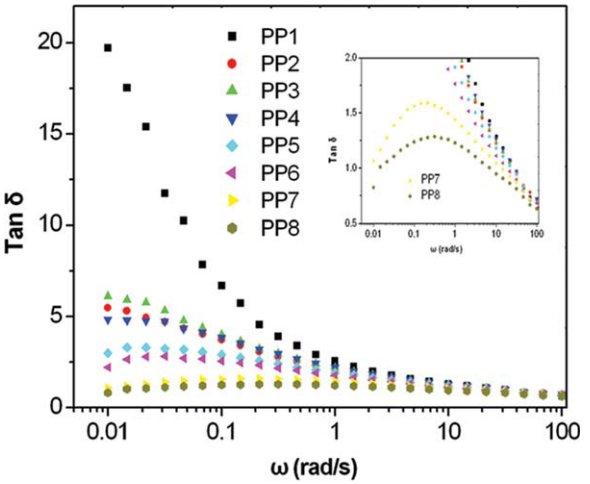

Figure 6 Tan δ vs. ω of linear PP, LCB-PP, LCB-PP/PP-g-MA blends, and LCB-PP/clay nanocomposites with varied clay concentrations at 190°C. [Color figure can be viewed in the online issue, which is available at wileyonlinelibrary.com.]

As shown in Figures 4–6, 2 phr clay cannot bring about significant differences in linear viscoelastic behavior between PP3 and PP4. This result demonstrates that a minimum amount of exfoliated platelets are needed to produce a visible increment in the elastic modulus or shear viscosity of the molten composites. In the present research, this minimum concentration of clay is about 2 phr when the concentration ratio of PP-g-MA to LCB-PP is fixed at 5 : 95. Similar results have been found in linear PP/clay nanocomposites, as reported by Quinzani and coworkers.[16] As the clay loadings increases above 4 phr (PP5-PP8), the values of G' in the low-frequency region are much higher than that of the LCB-PP resin (PP2), as shown in Figure 4. The so-called non terminal behavior in the G'-ω curve is observed in all nanocomposites when clay loading is above 4 phr. The non terminal behavior in the G'-ω curve becomes more notable with increasing clay loadings. As shown in Figure 5, the increase in clay concentration contributes to an increase in the complex viscosity of the composites at low-frequency. The shear-thinning behavior starts early at low-frequency, increasing clay concentration. Figure 6 shows that all nanocomposites exhibit a platform in the tan δ-ω curves in the high frequency regime, especially for PP6-PP8. The decreasing level of tan δ at low-frequency is proportional to the clay concentration. From Figures 4 and 6, it can be concluded that both the elastic modulus and the viscous modulus increased with an increase in clay concentration. Increment of the elastic modulus is larger than that of the viscous modulus with increasing clay concentration due to the formula tan $\delta = G''/G'$, and this effect is more noticeable at low-frequencies where tan δ gradually decrease with increasing clay concentration.

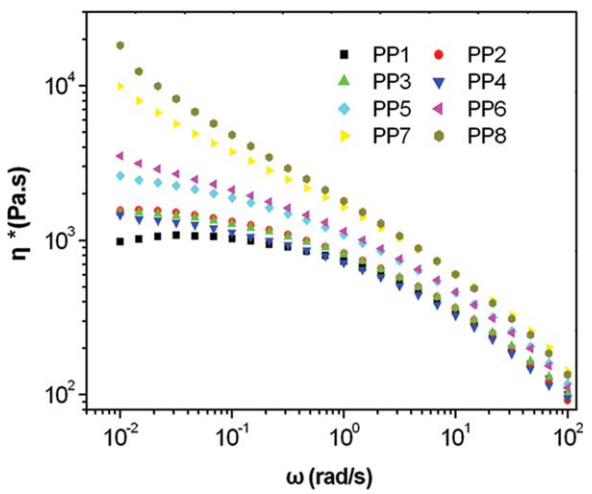

Figure 5 η* vs. ω of linear PP, LCB-PP, LCB-PP/PP-g-MA blends, and LCB-PP/clay nanocomposites with varied clay concentrations at 190°C. [Color figure can be viewed in the online issue, which is available at wileyonlinelibrary.com.]

These results suggest that a compact and stable filler network structure is constructed in these prepared nanocomposites when clay loading is high (4 phr).[12,16] The relaxation and mobility are substantially retarded by the confined spacing of the layered clay particles when a clay loading reaches a threshold value to form a percolated clay network. The analytical results from Figures 4 to 6 indicate that the influence of clay on the linear viscoelastic properties of LCB-PP is similar to clay's effect on the linear viscoelastic properties of linear PP.[12,16] Quinzani Nd coworkers[16] have confirmed that the non terminal

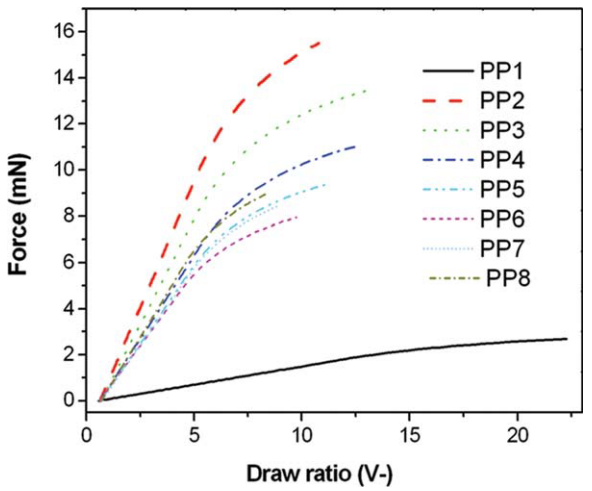

Figure 7 Melt elongation properties of linear PP, LCB-PP, LCB-PP/PP-g-MA blends, and LCB-PP/clay nanocomposites with varied clay concentrations at 190°C as observed by the Rheotens. (Data are fit according to the Wagner model). [Color figure can be viewed in the online issue, which is available at wileyonlinelibrary.com.]

behavior in the G'-ω curve becomes more notable as the extent of exfoliation increases and a compact and stable filler network structure was constructed in the linear PP/clay nanocomposites.

Elongation rheology of LCB-PP/clay nanocomposites

The materials response under elongational flow is highlighted in Figure 7, showing the experimental results of the Rheotens measurements at 190°C for linear PP, LCB-PP, LCB-PP/PP-g-MA blend, and LCB-PP/clay nanocomposites. Here, only the fitted data is shown for an improved clarity. The "melt strength" as the maximum force at the breakpoint of the melt strand, and the "drawability" denoting the maximum elongation at break, can directly be observed from the experimental data. The apparent elongational viscosity determined from the Rheotens data according to the Wagner model is shown in Figure 8. It is well-known that the sample's rheological history influences the experimental results, and this effect has been minimized by adjusting the die geometry and the experimental parameters.[21–23]

As shown in Figure 7, PP2 shows a pronounced improvement in melt strength and elongational viscosity, accompanied by a significant reduction in drawability, when compared to PP1. As reported by many researchers,[3,5] LCB-PP has a higher melt strength and elongational viscosity than linear PP when their molecular weights are equivalent, which is due to the existence of LCBs in the PP backbone. Moreover, it can be seen from Figure 7 that the melt strength and the drawability of LCB-PP are affected by the addition of clay. Interestingly, the melt strengths of all nanocomposites (PP4-PP8) are lower than that of the unfilled LCB-PP/PP-g-MA blend (PP3). The melt strength of nanocomposites decreases with increasing clay loading up to 6 phr and then slightly increases with further increases in clay concentration. The drawability of the nanocomposites decreases with increasing clay concentration.

Figure 8 shows that the elongational viscosity of the nanocomposites gradually decreases with increasing clay content up to 6 phr, and then slightly increases with further increases in clay concentration. Also, the elongational viscosity of nanocomposites is lower than that of the unfilled LCB-PP/PP-g-MA blend. A study on short glass fiber-filled polypropylene by Lin and Hu[10] has found that a higher elongational viscosity leads to a higher maximum draw-down force. Laun and Schuch[28] have suggested that low-elongational viscosity contributes to a reduction in the maximum draw-down force in melt spinning tests. Therefore, it can be concluded that the aforementioned change in the melt strength (see Fig. 7) results in the corresponding variation in the elongational viscosity for the LCB-PP/clay nanocomposites with increasing clay loadings.

McInerney et al.[7] have found that the melt strength of PP decreases when talcum is added at less than 40 wt % independent of testing conditions, and they confirmed that the drawability decreases with increased filler loadings. They thought that the reduction in melt strength with increasing talcum content was due to the degradation of the molecular weight of the PP matrix. This effect may be one reason for the decreasing melt strength of LCB-PP/clay nanocomposites with increasing clay loadings. LCB-

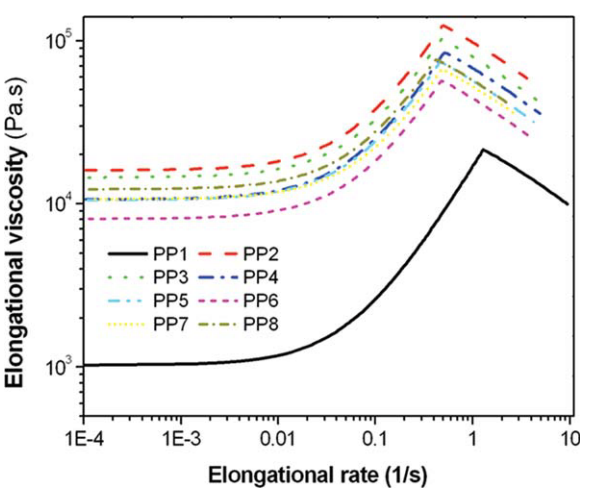

Figure 8 Apparent elongational viscosity determined from the Rheotens data according to the Wagner model for linear PP, LCB-PP, LCB-PP/PP-g-MA blends, and LCB-PP/ PP-g-MA/clay nanocomposites with varied clay concentrations at 190°C. [Color figure can be viewed in the online issue, which is available at wileyonlinelibrary.com.]

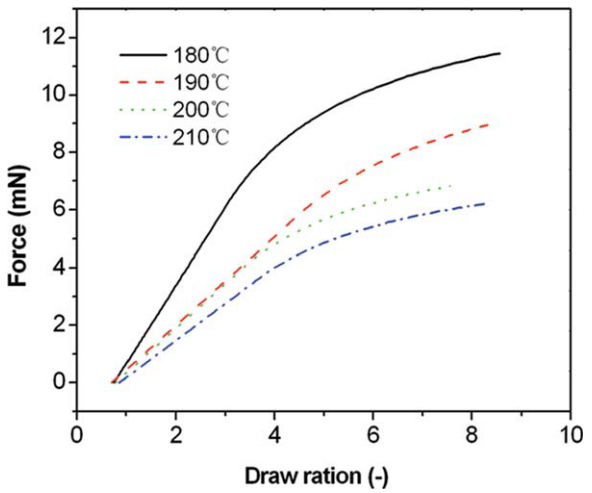

Figure 9 Melt elongational properties of PP8 at different extrusion temperature as observed by the Rheotens. (Data are fit according to the Wagner model). [Color figure can be viewed in the online issue, which is available at wileyonlinelibrary.com.]

PP and clay were compounded in a high-intensity mixing process. Then, the nanocomposites were prepared by melt blending in an extruder, which might result in the degradation and, subsequently, a reduction in the molecular weight of the LCB-PP matrix. However, this effect is not the sole reason for the decrease in melt strength with increasing clay concentration observed in these nanocomposites. When the clay platelets are dispersed in the LCB-PP matrix, they build up a network-like structure because of the intercalation of the LCB-PP molecular chains into the clay layers. Therefore, the improved level of melt strength and elongational viscosity caused by the LCB structure are minimized due to the intercalation of long-branching chains into the clay layers, explaining why the melt strength and elongational viscosity of the nanocomposites are lower than that of the neat LCB-PP. However, at higher clay loadings, the amount of long-branching chains intercalating the clay layers decreases because the clay platelets are not homogeneously dispersed in the polymer matrix. Therefore, the melt strength and elongational viscosity slightly increase in nanocomposites with clay loadings above 8 phr.

To investigate the temperature dependence on the melt strength and elongational viscosity for LCB-PP/clay nanocomposites, the melt extension and apparent elongational viscosity of PP8 as a function of extrusion temperature are shown in Figures 9 and 10, respectively. These graphs show that the melt strength and the elongational viscosity of PP8 exhibit similar variations with increasing extrusion temperature, which is due to low-elongational viscosity leading to a reduction in the maximum draw-down force in melt spinning tests.[10,28] The melt strength and elongational viscosity of PP8 decrease with increasing extrusion temperature. Increases in melt strength for PP melt with decreasing extrusion temperatures are attributed to flow-induced crystallization, as reported by Mcinerney et al.[7] In the present research, a sharp increase in the melt strength and elongational viscosity for LCB-PP/clay nanocomposites at low-extrusion temperatures approaching the melting point of PP might also be caused by flow-induced crystallization.

CONCLUSIONS

In this work, the microstructure and rheological behavior of LCB-PP/clay nanocomposites prepared by melt blending in an extruder were investigated using XRD, TEM, oscillatory shear rheology, and an elongational flow testing unit. Evidence from XRD and TEM confirms that the clay layers are intercalated by LCB-PP molecular chains, and the intercalated clay are well exfoliated in these nanocomposites. However, excessive clay in the system is harmful to the dispersion of clay in the LCB-PP matrix. A number of rheological properties, such as high storage modulus at low-frequency, high complex viscosity at low-frequency, a solid-like plateau in tan δ-ω curve, and increased shear-thinning behavior, appear in LCB-PP/clay nanocomposites as the concentration of clay reached a threshold level. The linear viscoelasticity of the nanocomposites suggests the formation of compact and stable filler network structure in the nanocomposites and emphasizes the important role played by the clay in the formation of this structure. The uniaxial elongational flow reveals that the melt strength and elongational

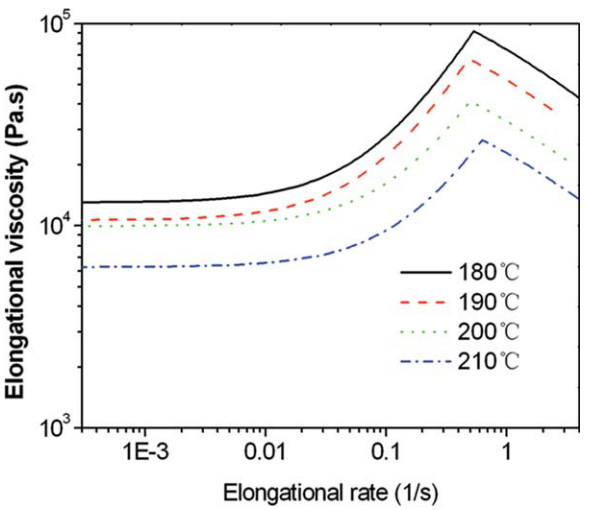

Figure 10 Apparent elongational viscosity determined from the Rheotens data according to the Wagner model of PP8 at different extrusion temperatures. [Color figure can be viewed in the online issue, which is available at wileyonlinelibrary.com.]

viscosity of the LCB-PP/clay nanocomposites decrease with increasing clay loading up to 6 phr and then slightly increase with further increases in clay loadings. This result may be caused by a reduction in the molecular weight of the LCB-PP matrix and by the intercalation of LCB-PP molecular chains into the clay layers.

References

1. Park, C. B.; Cheung, L. K. Polym Eng Sci 1997, 37, 1.
2. Nam, G. J.; Yoo, J. H.; Lee, J. W. J Appl Polym Sci 2005, 96, 1793.
3. Lagendijk, R. P.; Hogt, A. H.; Buijtenhuijs, A.; Gotsis, A. D. Polymer 2001, 42, 10035.
4. Graebling, D. Macromolecules 2002, 35, 4602.
5. Su, F. H.; Huang, H. X. Polym Eng Sci 2010, 50, 342.
6. Wong, B.; Bakert, W. E. Polymer 1997, 38, 2781.
7. Mcinerney, L. F.; Kao, N.; Bhattacharya, S. N. Polym Eng Sci 2003, 43, 1821.
8. Baldi, F.; Franceschini, A.; Bignotti, F.; Tieghi, G.; Riccó, T. Rheol Acta 2009, 48, 73.
9. Devendra, R.; Hatzikiriakos, S. G.; Vogel, R. J Rheol 2006, 50, 415.
10. Lin, G. G.; Hu, M. C. Adv Polym Technol 1997, 16, 199.
11. Li, P. Y.; Song, G. J.; Yin, L. N.; Wang, L.; Ma, G. P. J Appl Polym Sci 2008, 108, 2116.
12. Wang, K.; Liang, S.; Zhao, P.; Qu, C.; Tan, H.; Du, R.; Zhang, Q.; Fu, Q. Acta Mater 2007, 55, 3143.
13. Gopakumar, T. G.; Lee, J. A.; Kontopoulou, M.; Parent, J. S. Polymer 2002, 43, 5483.
14. Qiao, X. Y.; Zhong, W. X.; Sun, K.; Chen, X. D. J Appl Polym Sci 2009, 114, 2116.
15. Lee, J. W.; Kim, M. H.; Choi, W. M.; Park, O. O. J Appl Polym Sci 2006, 99, 1752.
16. Rohlmann, C. O.; Failla, M. D.; Quinzani, L. M. Polymer 2006, 47, 7795.
17. Sun, T. C.; Dong, X.; Du, K.; Wang, K.; Fu, Q.; Han, C. C. Polymer 2008, 49, 588.
18. Ding, C.; Jia, D. M.; Guo, B. C.; Hong, H. Q. Polym Test 2005, 24, 94.
19. Meissner, J. Rheol Acta 1971, 10, 230.
20. Muke, S.; Ivanov, I.; Kao, N.; Bhattacharya, S. N. J Non-Newtonian Fluid Mech 2001, 101, 77.
21. Wagner, H. M.; Bernnatm, A. J Rheol 1998, 42, 917.
22. Wagner, H. M.; Schulze, V.; Göttfert, A. Polym Eng Sci 1996, 36, 925.
23. Wagner, H. M.; Collignon, B.; Verbeke, J. Rheol Acta 1996, 35, 117.
24. Muke, S.; Ivanov, I.; Kao, S. N. Polym Int 2001, 50, 515.
25. Chapman, F. M.; Lee, T. S. SPE J 1970, 26, 37.
26. Mutel, A. T.; Kamal, M. R. Polym Compos 1984, 5, 29.
27. Suh, C. H.; Whitte, J. L. J Non-Newtonian Fluid Mech 1996, 62, 175.
28. Laun, H. M.; Schuch, H. J Rheol 1989, 33, 119.